

Buffer-gas cooling of atomic and molecular beamsDima Egorov,¹ Thierry Lahaye,^{1,*} Wieland Schöllkopf,¹ Bretislav Friedrich,^{1,2} and John M. Doyle¹¹*Department of Physics and Harvard-MIT Center for Ultracold Atoms, Harvard University, Cambridge, Massachusetts 02138*²*Department of Chemistry and Chemical Biology, Harvard University, Cambridge, Massachusetts 02138*

(Received 19 April 2002; published 4 October 2002)

We demonstrate direct loading and cooling of a thermal beam into a cryogenic helium buffer gas. Our test species is rubidium; we observe a thermal beam with $3 \times 10^{13} \text{ s}^{-1}$ flux entering a cryocell and thermalizing with a 4.2-K buffer gas. There is no evidence of clustering or other spurious loss mechanisms. The cooling technique should be applicable to a wide variety of species, including radicals.

DOI: 10.1103/PhysRevA.66.043401

PACS number(s): 33.80.Ps, 32.80.Pj, 39.10.+j

I. INTRODUCTION**A. Physics and chemistry with cold molecules**

The ability to cool and trap atoms set atomic physics on a new course marked by milestone experiments such as the observation of Bose-Einstein condensation [1], Fermi degeneracy [2] in a gas, superfluidity in atomic vapors [3], atom lasers [4], and nonlinear atom optics [5–7]. The challenge in molecular physics is to achieve with molecules what has so far been limited to atoms. This prospect is perhaps even more appealing, since molecules offer a vast range of properties not available with atoms. Unlike atoms, molecules are generally nonspherical and have rotational and vibrational degrees of freedom. Apart from that, molecules possess both even and odd multipole moments—electric and magnetic—that are all coupled to the rotating molecular frame. As a result, any molecular interaction, whether with other molecules or with external fields, is shaped and refined by a transformation between the rotating molecular frame and the space-fixed laboratory frame.

Cooling and trapping of molecules can produce a number of significant benefits for a wide variety of applications. Availability of reduced line broadening and long interaction times can benefit precision spectroscopy [8] and coherent control [9]. Cooling of internal molecular states, combined with long interaction times, can greatly increase the sensitivity of certain precision measurements [10]. Low translational energy of the cooled molecules will facilitate external-field manipulations of molecular trajectories and orientations [11–13]. In the regime where the de Broglie wavelength exceeds molecular dimensions, reactive collisions start exhibiting significant quantum effects [14]. Reactive and nonreactive collisions of ultracold molecules are of significant interest [15,16]. Beyond collisional properties, proposals exist for employing electric dipoles of ultracold molecules to implement quantum computing [17]. Finally, achieving quantum degeneracy with molecules remains a prominent goal. It will greatly expand the scope for study of collective quantum phenomena. For example, ensembles of polar molecules would constitute a system of relatively strongly interacting particles. In a Fermi-degenerate gas of polar molecules, the

electric dipole-dipole interaction, which is predicted to be energy independent [18–21], may give rise to a molecular superfluid via BCS pairing.

B. Cooling of molecules—previous work

Laser cooling and evaporative cooling have been the quintessential techniques for producing ultracold atoms. Evaporative cooling may be expected to work with molecules as well, provided their (yet unknown) elastic and inelastic low-temperature collisional cross sections are similar to those of atoms. Laser cooling of molecules, however, appears quite difficult, as the requisite closed-cycle transitions are generally not available due to the complex rovibrational level structure [22]. Four alternative techniques of cooling molecules, based on other principles, have been successfully implemented. (1) *Buffer-gas cooling* relies on thermalization of molecules with a cold He buffer gas; about 10^8 CaH molecules, produced by laser ablation inside a buffer-gas cell, were cooled to 400 mK and confined in a magnetic trap [23]. (2) *Stark deceleration* takes advantage of the adiabatic increase of Stark energy of polar molecules in an electrostatic field; up to 10^8 CO or ND₃ molecules produced by a pulsed supersonic expansion were slowed down to a standstill and confined in an electrostatic trap at a temperature of about 30 mK [24] and, more recently, in a storage ring [25]. (3) *Photoassociation of ultracold alkali-metal atoms* has been demonstrated to produce up to 10^6 dialkali-metal molecules at temperatures in the microkelvin range [26–28]. (4) *Supersonic expansion from a counter-rotating nozzle* has been demonstrated to produce 9 K molecules in the laboratory frame [29]. Also, slowing molecules using a laser scoop has been recently proposed [30,31].

Buffer-gas cooling is a very powerful technique. It is versatile and applicable to any atom or molecule, since it relies solely on elastic scattering cross sections. In addition, cooling of the translational degrees of freedom in the buffer gas is accompanied by efficient rotational cooling [32]. However, past implementations of the method have suffered from significant drawbacks, primarily difficulties connected with the introduction of the species of interest into the buffer gas.

In our previous buffer-gas work, laser ablation [32] was used to introduce the species of interest into the buffer-gas cell. In work by others, capillary filling [33–36] was used. Both techniques suffer from significant drawbacks. Laser ab-

*Permanent address: Département de Physique, École Normale Supérieure, 24 Rue Lhomond, 75230 Paris, France.

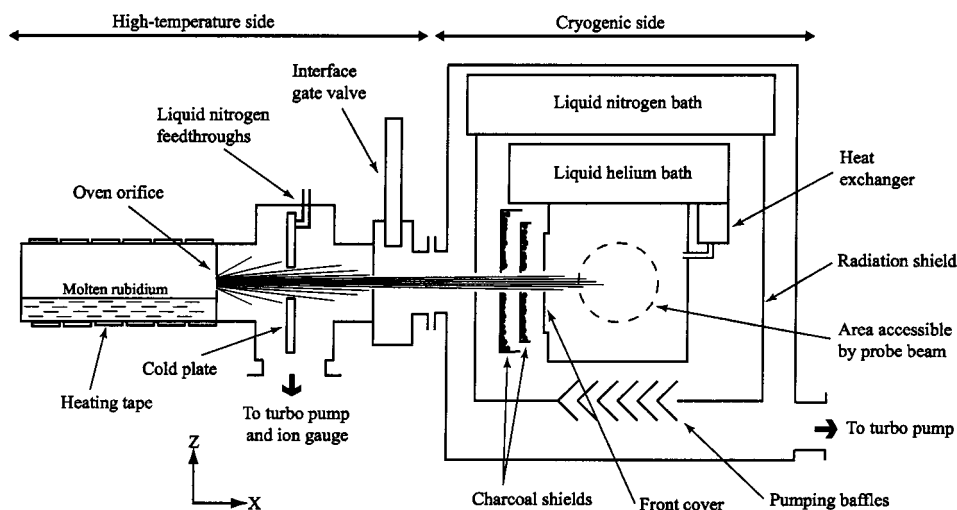


FIG. 1. Schematic view of the apparatus. Diameter of the oven orifice is 3.9 mm. Diameter of the orifice in the cell front cover was varied between 0 and 3 mm. Distance between oven orifice and cell orifice is 25 cm.

lation requires a suitable solid precursor, which is not always easily found. One is often forced to rely on the breakdown of more complex precursor molecules. For certain types of precursor, rapid destruction of the precursor pellet may occur (turning the pellet into dust, “drilling” a hole into it, etc.) [10]. The ablation process usually lacks specificity and unwanted species, including clusters, often form as by-products. If these react with or adsorb the species of interest, its population may be dramatically depleted [37]. Also, the yield of the molecules of interest per ablation pulse is limited and hard to predict (however, for certain precursors under suitable conditions, the yield per pulse can be quite constant [10]). Finally, ablation pulses bring additional heat into the cryogenic cell. Capillary filling suffers from small fluxes (needed to prevent clogging) and is difficult to implement in a cryogenic environment for species whose vapor pressure needs to be raised by heating [38]. Capillary filling of radicals is all but impossible.

C. Beam-based loading—this work

In this article we describe a proof-of-principle experiment that demonstrates loading of a cryogenic buffer-gas cell maintained at 4.2 K with a beam of rubidium atoms and thermalization of the atoms with the buffer gas. This beam-based method offers the following advantages: (1) It is versatile—atomic- and molecular-beam sources for a variety of atoms and molecules, including radicals, metastable species, and room-temperature solids, are available [39,40]; (2) fluxes as large as 10^{15} s^{-1} entering the cell can be expected from high-intensity beam sources, potentially leading to trapping of more than 10^{14} molecules (or atoms) using buffer-gas trapping techniques [32]; (3) beam sources make it possible to eliminate or to control the formation of clusters or other unwanted species; (4) for many gases and the low-melting-point solids, sources are simple in design and inexpensive; (5) multiple sources can be operated so as to introduce a combination of species into the buffer gas.

We first describe the experimental apparatus and procedure (Sec. II). Next we present the results of the measurements of the molecular-beam flux, steady-state density, and temperature in the cryocell and compare them with results of

a simple diffusion model (Sec. III). Finally, we discuss some prospective applications of the technique (Sec. IV).

II. EXPERIMENT

The apparatus, shown in Fig. 1, consists of two main parts, one cryogenic and one at high temperature. These are interfaced via a gate valve. The cryogenic part is based on a small liquid-nitrogen-shielded liquid-helium cryostat with a 1.2 l helium bath [41]. A cylindrical brass cryocell is thermally anchored to the liquid-helium bath. The cryocell is 10 cm long, and has an outer diameter of 6 cm and an internal volume $V = 150 \text{ cm}^3$. The side of the cell facing the interface gate valve has a thin replaceable front cover, made out of copper, mounted on an indium seal. The front cover has a circular orifice (cell orifice) whose diameter could be varied from 0 up to 3 mm. The molecular beam enters the cell through this orifice. At the same time, the He buffer gas leaks out through the cell orifice. A heat exchanger, made out of copper tubing [42], is mounted on the cryostat cold plate. The outlet of the heat exchanger is connected to the cell; the inlet (at room temperature) to an external gas-handling system via a 1.1 mm inner diameter stainless steel tube. The gas-handling system supplies helium gas (99.999% purity) at an adjustable steady rate such that the helium pressure in the cell remains constant (balanced by the helium leaving through the cell orifice). The heat exchanger ensures that the He gas entering the cell has the temperature of the liquid-helium bath. The cryocell is equipped with a pair of windows which enable optical access to the cell region. The temperature of the cell is monitored by silicon diode thermometers, and the pressure inside the cell by a Pirani gauge [43].

The liquid-helium bath and the cell are surrounded by a radiation shield connected to a liquid-nitrogen bath. Two charcoal shields [44] are placed between the cell orifice and the liquid-nitrogen shield to pump the He which leaks out from the cell orifice. The inner shield is thermally linked to the cell, the outer shield to the liquid helium bath. Most of the leaking He atoms are pumped by the inner shield and thus cannot reach the liquid-nitrogen radiation shield; those that do are likely to hit the outer charcoal shield after they

bounce back. The heat imparted to the He atoms by the liquid-nitrogen shield is then deposited in the liquid-helium bath and does not increase the temperature of the cryocell. Charcoal saturation can be a problem for very high He flow rates, so resistive heaters are placed on the shields to regenerate the charcoal if necessary. Under typical operating conditions, saturation does not occur for many hours, as expected [45]. When saturation occurs, the shields quickly overheat and self-regenerate, so the system is back in operation within minutes.

While charcoal cryopumping is effective in preventing heating of the cryocell, the probability of a helium atom sticking to charcoal in a single collision is less than unity. Therefore, some atoms will bounce multiple times and reach regions of the cell that are not protected by the shields. Due to design constraints, it was not practical to increase the shield coverage area. Instead, we enhanced the system's pumping speed with a turbomolecular pump. The bottom of the radiation shield is fitted with optically opaque baffles, which allow helium gas to pass through. The total estimated pumping speed from the turbopump-based part of the system is 100 l/s. We found that, even with no optimization of the charcoal shield or baffle designs, the thermal load due to a typical buffer-gas flow was constrained to under 2 mW, which is acceptable for a 4.2-K setup. Our simple design is not limited to liquid-helium temperatures, however: in a pumped ^4He or ^3He system, the cryocell could be protected with an additional radiation shield kept at 4.2 K. Since helium atoms would bounce back from a lower-temperature surface, heat loads would be dramatically reduced, allowing very low-temperature operation. We are currently constructing an apparatus based on the above design aimed to operate at a temperature of 1.2 K.

The high-temperature part of the apparatus consists of an oven and a collimation chamber. The front wall of the oven has a 3.9-mm-diam orifice. The distance between the orifice and the front of the cryocell is 25 cm. The oven is loaded with rubidium and heated up to about 350 °C (measured by thermocouples). The temperature of the oven is nonuniform, with measured temperature differentials between different surface points of up to 30 °C. We used the reading of the thermocouple closest to the oven orifice as the nominal oven temperature. With increasing oven temperature, the Rb flow changes from effusive toward hydrodynamic; we use less than 10^{-3} sr of the beam. A recirculating source might be a better choice for a long-term operation [46].

The collimation chamber, located between the oven and the interface gate valve, is fitted with a connection to a turbo pump and a cooled (160 K) condenser plate (placed about 6 cm downstream from the oven orifice). The plate has an 8-mm-diam aperture to collimate the beam. As the flux of the atoms out of the oven increases with increasing temperature, the pressure in the chamber rises above 10^{-4} mbar (the upper limit of our gauge). We did not observe any reduction of the beam flux into the cryocell due to high background pressure in the chamber. This type of setup was used in the case of rubidium because it reacts violently, and thus it is necessary for practical reasons to prevent its accumulation in the cryostat. For many other species the differential pumping

cold plate would not be necessary.¹

We measured the temperature and density of the Rb atoms in the cell using $5^2S_{1/2}, F=2 \rightarrow 5^2P_{3/2}, F'=1,2,3$ hyperfine transitions of the strong D_2 absorption line of ^{87}Rb (natural abundance of 27%) at 780 nm. The separations of these lines are the largest among the four D_2 hyperfine triplets of both Rb isotopes [47]; thus the overlap of Doppler-broadened lines at 4.2 K is avoided. The natural linewidth of the transitions of about 6 MHz is about a factor of 10 smaller than the 4.2-K Doppler broadening. Thus, the translational temperature of the Rb atoms could be accurately determined from fitting the measured line profiles to Voigt line shapes. Our laser source has a typical linewidth of 1 MHz and a Gaussian intensity profile with a 0.9 mm e^{-2} width. The laser beam is split among a single-mode fiber transmitting several microwatts to the cryocell, a wavemeter, and a saturation absorption setup used for calibrating both the wavelength and the optical density [48]. The cryostat is fitted with a platform which consists of a fiber out-coupler and a photodiode mounted on an X - Z translation stage (X is the direction of the Rb beam, Y the direction of the probe laser beam). This allows the probe beam to address points inside the cell anywhere within the 30-mm-diam cell window. The laser frequency can be scanned over 1 GHz. The photodiode signal was averaged typically over 30 scans per data point. Baseline subtraction was accomplished by blocking the Rb beam. The sensitivity of the absorption measurement was better than 10^{-3} .

III. RESULTS

In order to test and characterize the beam-loading technique, we carried out a series of experiments in which we determined the effects of buffer-gas density and oven temperature (molecular-beam flux) on the Rb number density. We also measured the spatial Rb-density distribution throughout the cryocell and determined the temperature of the Rb atoms within the cell. The results of these experiments are described and discussed below.

A. Effect of buffer-gas density

The loading process is sensitive to the density of the buffer gas. If the density is too low, the molecular beam will not be thermalized. If the density is too high, the molecules will thermalize too close to the cell entrance and a significant fraction of them will hit the cell front cover, stick to it, and thus be lost. Also, the buffer gas emerging from the cell will scatter the molecules and thus diminish their flow into the

¹We note that in the case of a 650-K oven coupled to a 4-K cryostat, thermal radiation propagating from the oven along the beam path does not pose a problem. However, if a lower loading temperature is desired and a ^3He cryostat or a dilution refrigerator has to be used, or in the case of significantly higher oven temperatures, heating by thermal radiation can no longer be neglected. A solution would be to use a pair of cooled chopper disks with non-overlapping slits that allow the beam pulses to pass through, but completely block the thermal radiation.

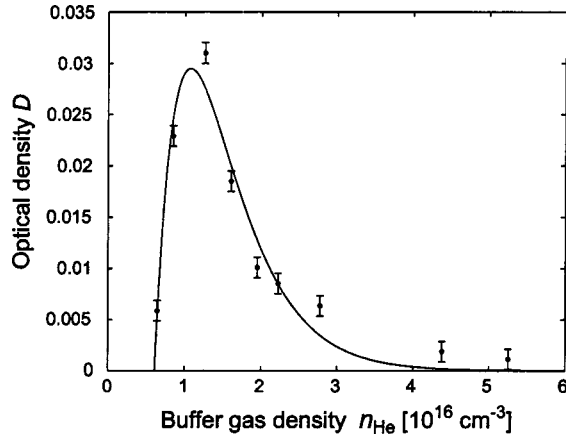


FIG. 2. Observed optical density of Rb atoms at the center of the cell held at a temperature of 4.3 ± 0.1 K as a function of buffer-gas density. All data points correspond to a complete thermalization. From the best fit of Eq. (6) (line) the optimal buffer-gas density for our cell configuration is $1.2 \times 10^{16} \text{ cm}^{-3}$, with an uncertainty of about 30%. The maximum total number of cold Rb atoms achieved was 1×10^{12} .

cell. At the outset, it was not clear whether an optimum balance (i.e., all of the Rb within the solid angle of the entrance orifice enters the cell) could be achieved. Therefore, we first established the dependence of the number density of the Rb atoms loaded into the buffer-gas cell on the buffer-gas density. The results are presented in Fig. 2. The absorption signal, proportional to the Rb number density, was measured at the center of the cell. At very low buffer-gas densities (or with no buffer gas), the absorption signal is strong, due to the collimated and unattenuated Rb beam inside the cell; the signal drops rapidly as the probe beam is moved away from the cell center along the z direction. Data points corresponding to such low buffer-gas densities are excluded from Fig. 2, since in that case no thermalization with the buffer gas takes place. All the data points shown correspond to full thermalization of the Rb atoms (see below). As seen in Fig. 2, the Rb density first sharply increases, reaches a maximum at about $n_{\text{He}} \approx 1.2 \times 10^{16} \text{ cm}^{-3}$, and levels off with increasing n_{He} . This distinctive behavior can be accounted for by a simple gas-kinetic model, used to fit the data in Fig. 2.

For an effusive flow from a uniformly heated oven at a temperature T_0 , the flux is

$$\Phi_0 = \frac{1}{4} n_0 v_0 A_0, \quad (1)$$

with n_0 the Rb number density in the oven, $v_0 = \sqrt{8k_B T_0 / (\pi M)}$ the average Rb velocity, M the Rb mass, and A_0 the oven orifice surface area. This flux is cryopumped away except for a fraction that passes through the condenser plate aperture to form a Rb beam directed toward the cryo-cell. In the absence of the buffer gas, the Rb beam intensity I_0 intercepted by the cell's entrance aperture is

$$I_0 \approx \frac{\Phi_0}{2\pi L^2}, \quad (2)$$

where L is the distance between the oven orifice and the cell aperture. In the presence of the He buffer gas, there is a steady flow of He out of the cell toward the collimation chamber. This flow results in an average He number density \bar{n}_{He} inside the region shielded by the charcoal cups (and possibly beyond) which attenuates the Rb beam by a factor $\exp[-\bar{n}_{\text{He}} \Lambda \sigma]$, with Λ the effective length over which scattering occurs, and σ the Rb-He scattering cross section. As a result, the Rb beam intensity that reaches the cell is reduced to

$$I_c = I_0 \exp[-\bar{n}_{\text{He}} \Lambda \sigma], \quad (3)$$

yielding a number density $n_c = I_c / v_0$ at the cell entrance. The values of \bar{n}_{He} and Λ depend on the He flow, the pumping speed, and the geometry of the cell. In general, we assume that Λ is constant, and that $\bar{n}_{\text{He}} = B n_{\text{He}}$, with B a proportionality constant.

The number of thermalized Rb atoms inside the cryogenic cell, N_{Rb} , is given by the flux of the Rb atoms into the cell, $N_{\text{in}} = I_c A_c$ (with A_c the cell aperture surface area) and the diffusion time τ to the cell walls,

$$N_{\text{Rb}} = \dot{N}_{\text{in}} \tau. \quad (4)$$

Since the diffusion time $\tau \approx 3V^{2/3} \sigma n_{\text{He}} v_0^{-1}$, where V is the volume of the cell, the Rb number inside the cell becomes

$$N_{\text{Rb}} = A n_{\text{He}} \exp[-B n_{\text{He}} \Lambda \sigma] \quad (5)$$

with $A \equiv 3A_c I_0 V^{2/3} \sigma v_0^{-1}$. The functional form of Eq. (5) was fitted to the measured optical density $D \propto \bar{n}_{\text{Rb}} \propto N_{\text{Rb}} / V$. The actual functional form used was

$$D = a(n_{\text{He}} - c) \exp[-b(n_{\text{He}} - c)]. \quad (6)$$

The solid line in Fig. 2 corresponds to the fitting parameters $a = 0.174$, $b = 2.17$, and $c = 0.61$, with n_{He} in units of 10^{16} cm^{-3} . Despite the simplifications of the model the best fit reproduces the main features of the observed data well. It reaches a maximum at $n_{\text{He}}^{\text{max}} = b^{-1} + c$ corresponding to $n_{\text{He}}^{\text{max}} = 1.1 \times 10^{16} \text{ cm}^{-3}$. The value for c is larger than could be explained by an offset in the absolute reading of the pressure gauge; however, the model does not attempt to accurately describe the low-buffer-gas density, long-mean-free-path regime. The value of b corresponds to $n_{\text{He}} / \bar{n}_{\text{He}} \approx 20$, assuming $\Lambda = 1 \text{ cm}$ and $\sigma = 100 \text{ \AA}^2$, which is consistent with estimates for the pumping speed for He within the region shielded by the charcoal cups.

B. Effect of oven temperature

We also established the dependence of the number density of the Rb atoms loaded into the buffer gas on the oven temperature. The results are presented in Fig. 3 for a He buffer-gas number density of $1.2 \times 10^{16} \text{ cm}^{-3}$ and a cell temperature of 4.2 K. The beam is not purely effusive at the higher temperature used; e.g., at 368 °C, the vapor pressure of Rb is 10 mbar. However, the measured optical density $D \propto n_{\text{Rb}}$, which is proportional to the incoming flux, Eq. (4), can still

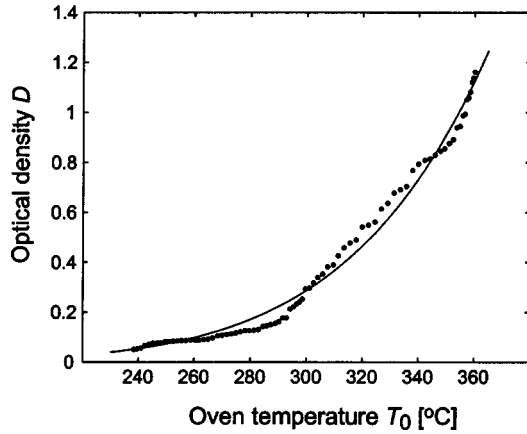


FIG. 3. Optical density of Rb atoms at the center of the cryogenic cell as a function of oven temperature. The cell temperature was 4.5 ± 0.5 K, buffer-gas density $1.5 \times 10^{16} \text{ cm}^{-3}$. The data were taken while the oven was slowly cooling down at a rate of about $0.1 \text{ }^\circ\text{C/s}$, to reduce effects due to nonuniform temperature distribution.

be well fitted by $D(T_0) = \alpha P_{T_0+T'}(T_0+T')^{-1/2}$, where $P_{T_0+T'}$ is the Rb vapor pressure inside the oven as a function of the effective oven temperature T_0+T' , with the coefficient of proportionality $\alpha = 2.5 \sqrt{\text{K/torr}}$. The value of the fitting parameter $T' = 26$ K might suggest that the effective oven temperature is larger by 26 K than the temperature indicated by the thermocouple. Initially, we expected to reach temperatures at which the flux in the forward direction stops increasing with increasing temperature, due to broadening of the angular distribution of the beam and cluster formation. However, we do not observe this effect up to the maximum oven temperature of $360 \text{ }^\circ\text{C}$. This indicates that the Rb atom flux could be further increased by increasing the oven temperature. We did not observe any effects of the oven temperature or of the atom flux on the loading or thermalization efficiency.

C. Thermalization

The thermalization was determined from the measured absorption line shapes. Figure 4 shows sample spectra of rubidium in the cell with and without buffer gas. Several effects contribute to the total linewidth, such as pressure, intensity, and Doppler broadening.

The relation between the Doppler broadening and the Rb temperature is dramatically different for atoms in the beam and in the buffer gas. In the case of the beam atoms, the observed broadening is a measure of the transverse velocity, which can be smaller than the longitudinal velocity by a factor of several hundred. On the other hand, for the Rb atoms in the buffer-gas cell, the Doppler broadening is in fact an accurate measure of the atoms' temperature, since the directions of their velocity vectors are randomized. As shown in Fig. 4, without the buffer gas, the Rb beam, collimated to about 30 mrad , yields a nearly natural linewidth, corresponding to a subkelvin transverse energy spread. As the buffer-gas density is increased, the beam becomes spatially dispersed, the (still fast) atoms no longer move in the same direction,

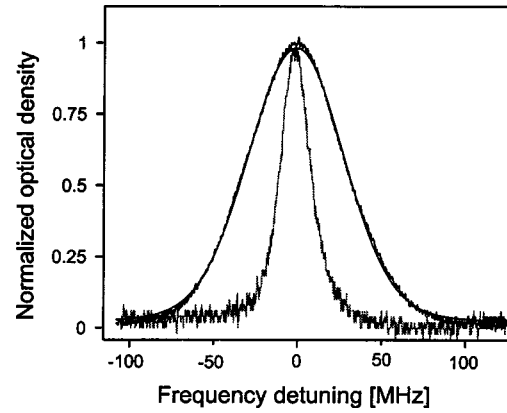


FIG. 4. Absorption line profile of rubidium inside the cell with (wide spectrum trace) and without (narrow spectrum trace) buffer gas. From the best fit of the Voigt profile (nearly overlapping the wide spectrum) the Rb temperature was determined to be 4.5 ± 0.3 K. The cell temperature was 4.3 ± 0.1 K, buffer-gas density $1.5 \times 10^{16} \text{ cm}^{-3}$, oven temperature $270 \pm 10 \text{ }^\circ\text{C}$.

and so the observed linewidth rapidly increases. At the same time, the absorption signal drops, due to a decrease of Rb number density in the probe region. As the buffer-gas density is further increased, the absorption signal begins to reappear, due to an increase of the diffusion time of Rb in the buffer gas. The linewidth narrows, reflecting the onset of thermalization. The linewidth approaches the value corresponding to the cell temperature at a buffer-gas number density of about 10^{16} cm^{-3} , and maintains this value at larger densities.

In fitting the measured line shapes to Voigt profiles, we fixed the contributions from the homogeneous broadening. This allowed us to extract the Doppler width and the temperature with a better accuracy. The pressure broadening was estimated from the data of Ref. [49]; the natural linewidth was taken from Ref. [48]. Moreover, since only a narrow range of buffer-gas densities, between 7×10^{15} and $3 \times 10^{16} \text{ cm}^{-3}$, leads to absorption signals large enough to make accurate fits, we did not observe an increase in pressure broadening over this range. The Rb temperature obtained from the fit of the data of Fig. 4 is 4.5 ± 0.3 K, close to the measured cell temperature of 4.3 ± 0.1 K. These data were taken at a buffer-gas density of $1.5 \times 10^{16} \text{ cm}^{-3}$ and oven temperature of $270 \pm 10 \text{ }^\circ\text{C}$. The Rb temperature across the field of view was uniform, consistent with conclusions from our Monte Carlo simulations and the model below.

The thermalization process can be modeled by assuming elastic collisions between two mass points m (^4He buffer-gas atom) and M (species to be cooled, i.e., ^{87}Rb in our case) [32]. From energy and momentum conservation in a hard-sphere model, after thermal averaging, the difference ΔT in temperature of the Rb atom before and after a collision with the He atom is given by $\Delta T = -(T_i - T)/\kappa$, with T the temperature of the buffer gas, T_i the kinetic energy of the Rb atom before the collision divided by the Boltzmann constant, and $\kappa \equiv (M+m)^2/(2Mm) \approx 12$. The temperature T_N corresponding to Rb atoms that had been at initial temperature T_0 and underwent N collisions each with the buffer-gas atoms is

$$T_N \approx (T_0 - T)e^{-N/\kappa} + T_0. \quad (7)$$

Therefore, in order for T_N to fall within 5% of $T \approx 4$ K, the Rb atoms have to undergo $N \approx 100$ collisions. In the course of the thermalization, the Rb atom will move over a distance

$$L_N \approx \frac{\sqrt{N}}{n_{\text{He}}\sigma}. \quad (8)$$

Assuming a Rb-He elastic cross section $\sigma \approx 50 \text{ \AA}^2$, $L_{N=100} \approx 0.2 \text{ cm}$ at $n_{\text{He}} \approx 10^{16} \text{ cm}^{-3}$. This is consistent with our observations: the probed region is about 10 mm downstream from the cell entrance where we find the Rb atoms thermalized.

D. Density distribution over the cryogenic cell

If all rubidium atoms are thermalized, the absorption signal is proportional to the integral of the rubidium number density along the laser beam, i.e., along the Y axis. To convert the signal into local rubidium densities or into the total number of atoms loaded, it is necessary to adopt a model of rubidium-density distribution. A Monte Carlo simulation of elastic collisions gives an accurate description of the loading process; however, due to significant computing time requirements it was used to process only a small fraction of the data. From our simulations we found that the range of input parameters that describes the optimal buffer-gas density corresponds to atoms entering the cell and thermalizing within several millimeters from the opening, and then diffusing across the cell into the probed volume. This behavior can be approximated by a diffusion equation with boundary conditions corresponding to absorption of particles at the walls, which is then used to convert the absorption data into number densities. Figure 5 shows comparisons of absorption signals at different locations in the cell with the predictions of the diffusion model. At the (optimal) buffer-gas density of $n_{\text{He}} = 1.5 \times 10^{16} \text{ cm}^{-3}$, a Rb density of $n_{\text{Rb}} = (8 \pm 4) \times 10^9 \text{ cm}^{-3}$ at the center of the cell is observed, indicating a total number of thermalized Rb atoms loaded into the cell of $N_{\text{Rb}} = (1 \pm 0.5) \times 10^{12}$. To determine F_c , the flux of Rb atoms entering the cell with no buffer gas present, we scanned the probe beam across the atomic beam inside the cell, and converted the absorption signal into F_c . In doing so, we took into account the Gaussian intensity profile of the laser beam and cylindrical symmetry of the atomic beam. We then introduced buffer gas into the cell, and measured the corresponding N_{Rb} . Due to technical limitations, we were able to perform this measurement only at low fluxes, up to the level $F_c = 5 \times 10^{11} \text{ s}^{-1}$, for which $N_{\text{Rb}} = 1.5 \times 10^{10}$. We assume, based on Eq. (4) above, that with increasing flux of Rb atoms N_{Rb} should not increase more rapidly than F_c . We therefore estimate the highest flux achieved in our experiment to be at least $F_c = (3 \pm 1.5) \times 10^{13} \text{ s}^{-1}$.

Based on the value for the Rb-He diffusion coefficient in Ref. [50] we estimate the scattering cross section σ at 4.2 K to be 50 \AA^2 , which gives the diffusion time $\tau \approx 100 \text{ ms}$. For $\tau = 100 \text{ ms}$ and $N_{\text{Rb}} = 1.5 \times 10^{10}$ we calculate, using Eq. (4), the number of Rb atoms entering the cell with the buffer gas

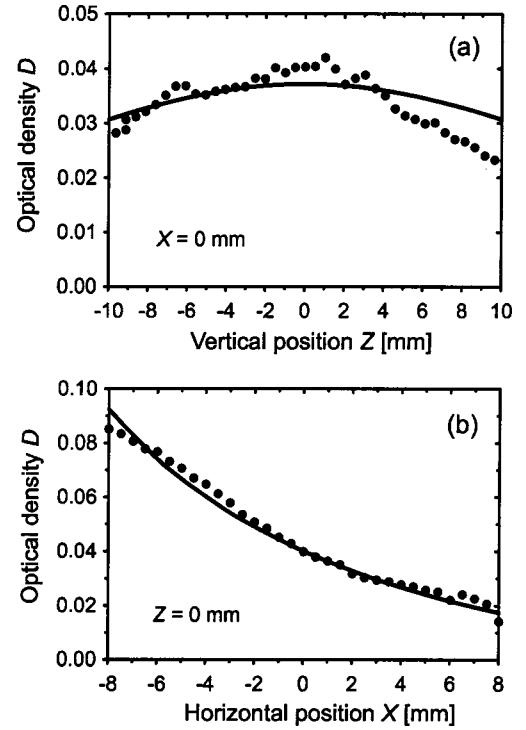


FIG. 5. Optical density of Rb atoms in the cell as a function of the probe-beam position. Circles are experimental data, lines are simulations based on the diffusion model; see text. The cell center defines the origin of the coordinate system. The cell temperature was $4.3 \pm 0.1 \text{ K}$, buffer-gas density $1.5 \times 10^{16} \text{ cm}^{-3}$. (a) Probe beam is scanned vertically along Z axis at $X = 0 \text{ mm}$. (b) Probe beam is scanned horizontally along X axis at $Z = 0 \text{ mm}$.

present as $\dot{N}_{\text{in}} = 1.5 \times 10^{11} \text{ s}^{-1}$. This number is approximately three times smaller than the measured number of atoms entering the cell with no buffer gas. This indicates that a significant fraction of Rb atoms coming toward the cell orifice are loaded into the buffer gas.

IV. PROSPECTS

Direct loading of a molecular beam into a cryogenic buffer-gas cell is a facile and efficient technique of cooling gaseous species. The apparatus described can be used to carry out a variety of spectroscopic measurements on atoms, molecules, radicals, and metastable species at cryogenic temperatures. The apparatus can be extended by adding another molecular beam, to study cold collisions and chemical reactions.

An exceptionally wide variety of atomic and molecular species can be produced in a molecular beam [39,40]. Since our technique makes no use of cooling due to the beam expansion, the only parameter of interest is the beam flux in the forward direction. As a result, a simple effusive source with modest pumping requirements may suffice; the stagnation pressure can, of course, be significantly increased if greater flux is required. Since the beam temperature is insignificant in our scheme, the source can be operated at as high a temperature as necessary for raising the vapor pressure or for enabling the generation of the species of interest. As a result,

any species that can form a molecular beam can be loaded into the cryogenic cell, including reactive species such as radicals.

The technique could also be used to load a magnetic trap enclosing the cell. We expect to be able to load and magnetically trap a large number of paramagnetic molecules. By applying evaporative cooling, the relatively high loading temperatures (between 0.24 and 1.2 K) could then be reduced to the millikelvin range or lower. An experiment is underway to trap $\text{NH}(X^3\Sigma^-)$ molecular radicals; we expect to load about 10^{12} NH molecules into a He buffer gas at 1.2 K, and then magnetically trap over 10^{11} of them. As the

technique is simple and versatile, many other applications are likely to emerge.

ACKNOWLEDGMENTS

We thank Mara Prentiss for providing the laser, and Siu Au Lee for helpful discussions. This work was supported by Harvard University and the National Science Foundation. We thank the National Science Foundation (D.E.) and the Alexander von Humboldt Foundation (W.S.) for partial financial support.

-
- [1] M. Anderson, J. Ensher, M. Matthews, C. Wieman, and E. Cornell, *Science* **269**, 198 (1995).
- [2] B. de Marco and D. Jin, *Science* **285**, 1703 (1999).
- [3] R. Onofrio, C. Raman, J. M. Vogels, J. Abo-Shaer, A. P. Chikkatur, and W. Ketterle, *Phys. Rev. Lett.* **85**, 2228 (2000).
- [4] M.-O. Mewes, M. R. Andrews, D. M. Kurn, D. S. Durfee, C. G. Townsend, and W. Ketterle, *Phys. Rev. Lett.* **78**, 582 (1997).
- [5] S. Inouye, T. Pfau, S. Gupta, A. P. Chikkatur, A. Gorlitz, D. E. Pritchard, and W. Ketterle, *Nature (London)* **402**, 641 (1999).
- [6] C. E. Wieman, D. E. Pritchard, and D. J. Wineland, *Rev. Mod. Phys.* **71**, S253 (1999).
- [7] S. E. Harris and L. V. Hau, *Phys. Rev. Lett.* **82**, 4611 (1999).
- [8] B. Friedrich, R. deCarvalho, J. Kim, D. Patterson, J. D. Weinstein, and J. M. Doyle, *J. Chem. Soc., Faraday Trans.* **94**, 1783 (1998).
- [9] R. J. Gordon and S. A. Rice, *Annu. Rev. Phys. Chem.* **48**, 601 (1997).
- [10] D. Egorov, J. D. Weinstein, D. Patterson, B. Friedrich, and J. M. Doyle, *Phys. Rev. A* **63**, 030501(R) (2001).
- [11] H. Stapelfeldt, H. Sakai, E. Constant, and P. B. Corkum, *Phys. Rev. Lett.* **79**, 2787 (1997).
- [12] A. Boca and B. Friedrich, *J. Chem. Phys.* **112**, 3609 (2000).
- [13] B. Friedrich and D. R. Herschbach, *Nature (London)* **353**, 412 (1991).
- [14] D. R. Herschbach, in *Chemical Research—2000 and Beyond: Challenges and Visions*, edited by P. Barkan (Oxford University Press, New York, 1998), p. 113.
- [15] N. Balakrishnan and A. Dalgarno, *Chem. Phys. Lett.* **341**, 652 (2001).
- [16] C. Zhu, N. Balakrishnan, and A. Dalgarno, *J. Chem. Phys.* **115**, 1335 (2001); J. L. Bohn, *Phys. Rev. A* **63**, 052714 (2001); J. L. Bohn, *ibid.* **62**, 032701 (2000); N. Balakrishnan, A. Dalgarno, and R. C. Forrey, *J. Chem. Phys.* **113**, 621 (2000); J. L. Bohn, *Phys. Rev. A* **61**, 040702 (2000).
- [17] D. DeMille, *Phys. Rev. Lett.* **88**, 067901 (2002).
- [18] M. Baranov, Y. Kagan, and M. Kagan, *JETP Lett.* **64**, 301 (1996).
- [19] M. Houbiers, R. Ferwerda, H. T. C. Stoof, W. I. McAlexander, C. A. Sackett, and R. G. Hulet, *Phys. Rev. A* **56**, 4864 (1997).
- [20] M. A. Baranov, M. S. Mar'enko, V. S. Rychkov, and G. V. Shlyapnikov, e-print cond-mat/0109437.
- [21] Y. Kagan, I. A. Vartanyants, and G. V. Shlyapnikov, *Sov. Phys. JETP* **54**, 590 (1981).
- [22] J. T. Bahns, W. C. Stwalley, and P. L. Gould, *J. Chem. Phys.* **104**, 9689 (1996).
- [23] J. D. Weinstein, R. deCarvalho, T. Guillet, B. Friedrich, and J. M. Doyle, *Nature (London)* **395**, 148 (1998).
- [24] H. L. Bethlem, G. Berden, F. M. H. Crompvoets, R. T. Jongma, A. J. A. van Roij, and G. Meijer, *Nature (London)* **406**, 491 (2000); G. Meijer (private communication).
- [25] F. M. H. Crompvoets, H. L. Bethlem, R. T. Jongma, and G. Meijer, *Nature (London)* **411**, 174 (2001).
- [26] P. Pillet, C. Drag, and B. L. Tolra, *Laser Phys.* **11**, 480 (2001), and references cited therein.
- [27] A. N. Nikolov, J. R. Ensher, E. E. Eyler, H. Wang, W. C. Stwalley, and P. L. Gould, *Phys. Rev. Lett.* **84**, 246 (2000), and references cited therein.
- [28] R. Wynar, R. Freeland, D. Han, C. Ryu, and D. Heinzen, *Science* **287**, 1016 (2000).
- [29] M. Gupta and D. Herschbach, *J. Phys. Chem. A* **105**, 1626 (2001).
- [30] B. Friedrich, *Phys. Rev. A* **61**, 025403 (2000).
- [31] B. Friedrich and D. Herschbach, *Phys. Rev. Lett.* **74**, 4623 (1995).
- [32] R. deCarvalho, J. M. Doyle, B. Friedrich, T. Guillet, J. Kim, D. Patterson, and J. D. Weinstein, *Eur. Phys. J. D* **7**, 289 (1999).
- [33] J. K. Messer and F. C. DeLucia, *Phys. Rev. Lett.* **53**, 2555 (1984).
- [34] D. R. Willey, R. L. Crownover, D. N. Bittner, and F. C. De Lucia, *J. Chem. Phys.* **89**, 1923 (1988).
- [35] J. C. Pearson, L. C. Oesterling, E. Herbst, and F. C. De Lucia, *Phys. Rev. Lett.* **75**, 2940 (1995).
- [36] M. M. Beaky, T. M. Goyette, and F. C. De Lucia, *J. Chem. Phys.* **105**, 3994 (1996).
- [37] J. D. Weinstein, R. deCarvalho, K. Amar, A. Boca, B. C. Odom, B. Friedrich, and J. M. Doyle, *J. Chem. Phys.* **109**, 2656 (1998).
- [38] P. Jin, H. Wang, S. Oatis, G. E. Hall, and T. J. Sears, *J. Mol. Spectrosc.* **173**, 442 (1995).
- [39] G. Scoles, *Atomic and Molecular Beam Methods* (Oxford University Press, New York, 1988).
- [40] H. Pauly, *Atom, Molecule, and Cluster Beams* (Springer, Berlin, 2000).
- [41] Infrared Laboratories HDL-5.
- [42] 1.7 mm inner diameter, 50 cm long.

- [43] The pressure in the cell is monitored by a Pirani gauge (Grainville-Phillips Convectron 250), connected to the cell via a straight stainless steel tube, 45 cm long and of a 1.9 mm inner diameter. The gauge is at room temperature, so a difference between the pressure reading and the actual pressure in the cryogenic cell can exist; see T. R. Roberts and S. G. Sydorik, *Phys. Rev.* **102**, 304 (1956). Also, helium gas flow may affect the pressure reading. By performing a number of measurements, such as the drop of pressure in a known-volume gas supply vessel and pressure measurements for different orifice openings with a ruthenium oxide sensor suspended inside the cell, we established that these effects fall within the absolute calibration uncertainty of the pressure gauge, and have no effect on its relative accuracy.
- [44] Thin copper cups with 20/40 mesh coconut activated charcoal (Supelco #10275) attached by epoxy.
- [45] D. W. Sedgley, A. G. Tobin, T. H. Batzer, and W. R. Call, *J. Vac. Sci. Technol. A* **5**, 2572 (1987).
- [46] M. R. Walkiewicz, P. J. Fox, and R. E. Scholten, *Rev. Sci. Instrum.* **71**, 3342 (2000).
- [47] E. Arimondo, M. Inguscio, and P. Violino, *Rev. Mod. Phys.* **49**, 31 (1977).
- [48] G. P. Barwood, P. Gill, and W. R. C. Rowley, *Appl. Phys. B: Photophys. Laser Chem.* **53**, 142 (1991).
- [49] M. V. Romalis, E. Miron, and G. D. Cates, *Phys. Rev. A* **56**, 4569 (1997).
- [50] A. Hatakeyama, K. Oe, K. Ota, S. Hara, J. Arai, T. Yabuzaki, and A. R. Young, *Phys. Rev. Lett.* **84**, 1407 (2000).